Journal of Physics and Chemistry of Materials **Research Paper**
Vol.5, Issue.1, pp.01-07, March (2018) **E-ISSN:** 2348-6341

A First Principle and Experimental study of Double Perovskite

Ashwani Kumar

Department of Physics, National Defence Academy, Khadakwasla, Pune - 411 023, MH, India

**Corresponding Author: ashwani_kumar04@yahoo.co.in*

https://doi.org/10.26438/jpcm/v5i1.17 | Available online at: www.isroset.org

Received: 04/Jan/2018, Accepted: 09/Mar/2018, Online: 31/Mar/2018

Abstract **-** Indium Zinc Titanate, $In_2(ZnTi)O_6$ (IZT), a double perovskite is synthesized. The field dependence of the conductivity and the dielectric response of the sample are measured in a wide frequency and temperature. It is observed that, the dielectric constant decreases with the increase of frequency. The frequency dependence of the loss peak is found to obey an Arrhenius law with activation energy of 0.73 eV. An analysis of loss factor with frequency is performed by using the scaling behaviour of the dielectric loss spectra. The complex impedance plot of the sample confirms that the polarization mechanism in IZT corresponds to bulk effect of semiconductor IZT particles. The relaxation mechanism is discussed in the framework of impedance and modulus formalism. The full potential linearized augmented plane wave method is employed to study the ground state properties.
PACS numbers: 71.15.Dx; 71.15.Mb; 71.20.-b; 77.22.-d

Keywords: Pseudopotential; Density Functional theory (DFT), Electronic density of states and band structure, Dielectrics

1. INTRODUCTION

Double perovskite oxides having chemical formula $A_2(B'B'')O_6$ are the subject of investigation during the recent years [1-5] due to their large potential applications. In this type of system, each transition metal site (B′B″) is surrounded by an oxygen octahedra and the A atoms site are situated in the holes produced by eight adjacent oxygen octahedra. The properties of double perovskite compounds are determined by the relative sizes, valencies and ordering of the A and B site ions.

The physics of double perovskites $A_2(B'B'')O_6$ is very rich as they are very flexible with respect to variations of the magnetic and/ or non-magnetic B′B″ ions as well as the A-site cations. A large increase in double perovskite research was initiated in 1998 with the discovery of large room temperature magneto resistive effects at low magnetic fields in Sr_2FeMoO_6 [6]. Thus the physics of double perovskites offers a wide range of possibilities to influence the structure and/or the magnetic interactions to tailor the electrical and/or magnetic properties for specific applications.

The state of ordering of the two B-site cations in the perovskite structure can be modified either by the application of suitable thermal treatment [7] or doping with various elements [8]. Retuerto *et al.* [9] have studied the crystal structure of Ca_2CrSbO_6 from powder X-ray diffraction data. Caracas *et al.* [10, 11] have studied the phonon dispersion relations for the high temperature cubic and low temperature average rhombohedral polymorphs of Pb_2MgTeO_6 (PMT) and have discussed the instabilities in the different phase. Both the cubic and rhombohedral structures are investigated using the local-density approximation (LDA) within the density functional theory (DFT). Baldinozzi *et al.* [12, 13] have investigated the crystal structure of the cubic phase of the complex perovskite Pb_2CoWO_6 by single crystal X-ray diffraction (XRD) and neutron powder diffraction. The phase transition in the elpasolite compound lead magnesium tellurate (PMT) has been characterized by calorimetry, dielectric permittivity measurements and Raman spectroscopy. Azad *et al.* [14] have studied the structural and magnetic properties of Ba_2MnWO_6. Battle *et al.* [15] have employed the powder neutron diffraction data to refine the crystal and magnetic structures of the ordered perovskites Sr_2LuRuO_6, Ba_2YRuO_6 and Ba_2LuRuO_6, Sr_2YRuO_6. Given the vast possibilities in variation of these parameters, interesting and useful physics is likely to appear from further studies of these classes of materials.

In the present work, we have prepared and investigated the dielectric properties of the double perovskite oxide indium zinc titanate In_2ZnTiO_6 (IZT) using impedance spectroscopy for the first time at ambient pressure conditions. Its ground state properties have also been studied employing full potential linearized augmented plane wave (FLAPW) method [16]. In the following sections, the experimental as well as the computational details and results have been discussed.

2. EXPERIMENTAL PROCEDURE

The material IZT was synthesized by the solid-state reaction technique. Powders of In_2O_3, ZnO and TiO_2 were taken in stoichiometric ratio and mixed in the presence of acetone

for 12 hours. The mixture was calcined in Pt. crucible at 1050 ^{0}C in air for 8 h and brought to room temperature under controlled cooling. The calcined sample was pelletized into a disc using polyvinyl alcohol (PVA) as binder. Finally, the discs were sintered at 1100^{0}C for 6 h and cooled down to room temperature by controlling the cooling rate.

The x-ray powder diffraction pattern of the sample was taken at room temperature using Philips PW1877 automatic x-ray powder diffractometer. For the dielectric characterization, the sintered disc (of diameter 9.14 mm and thickness 2.24 mm) was polished and then gold electrodes were evaporated onto both sides of the disc. The temperature and frequency dependence of the dielectric characterization was carried out using LCR meter (HIOKI). The dielectric permittivity ε' and the dielectric loss tangent $\tan\delta$ of the sample were measured in the frequency range from 42 Hz to 1.1 MHz and in the temperature range from room temperature to 673 K. The temperature was controlled with a programmable oven. All the dielectric data were collected while heating at a rate of 0.5 ^{0}C min^{-1}. These results were found to be reproducible.

3. RESULTS AND DISCUSSIONS

Fig. 1 shows the XRD pattern of the sample taken at room temperature and the phase appears to be cubic symmetry (*Fm3m*). Lattice parameters have been calculated by a least square fit to measured d-values. In **Fig. 2 (a)**, the angular frequency ω (= $2\pi\upsilon$) dependence of the dielectric constant ε' of IZT at various temperatures are plotted. The dielectric constant ε' decreases with the increase of frequency. In the presence of an alternating electric field; the dipole will experience a torque and hence will rotate itself in the reverse direction of the electric field causing orientation polarization to occur.

(a) At frequencies below relaxation, the dipoles managed to keep pace with the field variations. As the frequency increases, the storage ε' begins to decrease due to the phase lag between the dipole alignment and the electric field.

(b) Above the relaxation frequency, ε' drops off as the frequency of electric field is too fast to influence the dipole rotation and hence the orientation polarization disappears. The observation is shown in Fig. 2(a).

At the temperature 463 K, dielectric constant gradually decreases with increase in frequency, at the rate of 370 for 50 Hz. With increasing temperature, it increases apparently, which becomes even more significant at low frequency (below 200 Hz). At elevated temperatures (>633 K), the dielectric constant at low frequency is rather high (>2800), and it falls against frequency at first and then gets stabilized down to above 300 Hz (Fig.2 (a)). The high value of ε' at frequencies lower than 1 KHz increases with decreasing frequency and increasing temperature may be due to electrode polarization rising usually from space charge accumulation at the sample electrode interface. The resistance accompanying the orientation of the dipole will contribute to the dielectric loss. In **Fig. 2(b)**, the frequency dependence of the loss tangent of the sample IZT at various temperatures are plotted. The material shows the thermally activated nature of the dielectric relaxation as the $\tan\delta$ maximum decreases with the increase in temperature. The values of most probable relaxation time τ_m were obtained from the peak frequencies ω_m ($\omega_m\tau_m = 1$).

Fig. 3 represents a plot of ω_m Vs. 10^3 / T. The activation energy E_a calculated from least-square fit to the data points found to be 0.73 eV. Such a value of activation energy indicates that the conduction mechanism for the present system may be due to the polaron hopping based on electron carriers.

In **Fig. 4**, the $\tan\delta$ (ω, T) data in scaled coordinates, i.e., $\tan\delta$ (ω, T) / $\tan\delta_m$ and log (ω / ω_m) has been plotted. It is found that the entire dielectric loss data can be collapsed into one single curve. The scaling behaviour of $\tan\delta$ (ω, T) clearly indicates that the relaxation mechanism in IZT is nearly temperature independent. Here, ω_m corresponds to the frequency of the peak loss in the $\tan\delta$ Vs log ω plot.

In Fig.5, the frequency dependent a.c. conductivity plot has been shown at various temperatures. The conductivity follows the power law, according to which the real part of the a.c. conductivity is given as [17, 18]:

$$\sigma' = \sigma_{dc}\left[1+\left(\frac{\omega}{\omega_H}\right)^n\right] \qquad (2)$$

Where σ_{dc} is the dc conductivity, ω_H is the hopping frequency of the charge carriers, and n is the dimensionless frequency exponent. Equation (2) can be obtained from the imaginary part of the complex dielectric susceptibility [19]. The experimental conductivity data were fitted to Eq. (2) with σ_{dc} and ω_H as variables, keeping in mind that the values of parameter n are weakly temperature dependent. The best fit of the conductivity spectra is exhibited by solid lines in Fig. 5 at various temperatures. The reciprocal temperatures dependences of σ_{dc} are shown in **Fig. 6**, which indicates that σ_{dc} obey the Arrhenius relation. The value of the activation energy is found to be E_σ (= 0.72 eV).

Fig.7 represents the complex Argand plane plots between ε'' and ε' usually called Cole-Cole plots [20]. The complex dielectric constant is known to be classified by the empirical relation

$$\varepsilon^* = \varepsilon_\infty + \frac{(\varepsilon_s - \varepsilon_\infty)}{(1+j\omega T)^{1-\alpha}} \qquad (3)$$

where α is a measure of the distribution of relaxation times and is zero for monodispersive Debye process. The parameter α is obtained from the angle subtended by the radius of Cole-Cole circle with the ε'-axis passing through the origin of ε''-axis is found to be 0.1 at 633 K. The Cole-Cole plot confirms the polydispersive nature of dielectric relaxation of IZT.

Fig.8, shows the frequency (angular) dependence of M′ (ω) and M″(ω) for IZT as a function of temperature. M′ (ω) indicates the dispersion tending towards M_∞ (the asymptotic value of M′ (ω) at higher frequencies), while M″(ω) exhibits a maximum M''_{max} centered at the dispersion region of M′ (ω). From Fig. 8(b), it may be inferred that the position of the peak M''_{max} shifts to higher frequencies as the temperature is increased. The frequency region below the maxima of the peak determines the range in which carriers are mobile on long distances. At frequency above peak maximum M″, the carriers are confined to potential wells, being mobile on short distances. The frequency ω_m (corresponding to M''_{max}) gives the most probable relaxation time τ_m from the equation $\omega_m \tau_m = 1$.

Fig. 9 represents that the most probable relaxation time also obeys the Arrhenius relation and the corresponding activation energy $E_\tau = 0.74$ eV. In **Fig. 10**, the M''/M''_{max} at each frequency by ω_m has been scaled for different temperatures. The overlapping of curves onto a master curve signifies that the dynamical processes are nearly temperature independent.

Fig.11 shows the frequency (angular) dependence of impedance for IZT at various temperatures. It is evident from Fig.11 (b) that the peak value of Z″ decreases with increasing temperature and the peak position shifts to higher frequency side. At higher frequencies, all curves appear to merge. This may be attributed to the presence of space charges in the material. The decrease in the peak value of Z″ with the increase in temperature denotes the increase in capacitance and hence the decrease in resistance of the material which indicates the increase in conductivity. In such a situation, one can determine the most probable relaxation time τ_m (= 1 / ω_m) from the position of the peak in the Z″ Vs. log ω plots. The most probable relaxation time follows the Arrhenius law given by

$$\omega_m = \omega_0 \exp\left[\frac{-E_a}{k_B T}\right] \qquad (3)$$

where ω_0 is the pre-exponential factor and E_a is the activation energy.

Fig. 12 shows a plot of the log ω_m Vs. 1 / T, where the crosses are the experimental data and the solid line is the least-square straight-line fit. The activation energy E_a calculated from least squares fit to the points is 0.76 eV.

In **Fig. 13**, the Z″ (ω, T) data in scaled coordinates, i.e., $Z''(\omega, T) / Z''_{max}$ and log (ω / ω_m) has been plotted. Here ω_m corresponds to the frequency of the peak value of Z″ in the Z″ Vs. logω plots. It is found that the entire data of imaginary part of impedance overlap onto a single curve. The scaling behaviour of Z″ clearly indicates that the distribution of relaxation times is nearly temperature independent.

Fig.14 shows a complex-plane impedance plots. In this figure, the imaginary part of impedance, Z″ has been plotted against the real part of impedance, Z′. In general for a perfect crystal, the values of resistance R and capacitance C can be analyzed by an equivalent circuit of one parallel resistance-capacitance (RC) element. This RC element gives rise to one semicircular arc on the complex plane and has intercepts on the Z′-axis of zero and R. Thus, C can be calculated with the relation $\omega_m RC = 1$, where $\omega_m = 2\pi\nu_m$ and ν_m is the frequency at the arc maxima. For a bulk crystal containing interfacial boundary layers, the equivalent circuit may be considered as two parallel RC elements connected in series and it gives rise to two arcs in complex plane viz., one for bulk crystal (grain) and the other for the interfacial boundary (grain-boundary) response. The arc of the bulk generally lies on frequency range higher than that of interfacial boundary since the relaxation time $\tau_m = 1 / \omega_m$ for the interfacial boundary is much larger than that for the bulk crystal. The absence of any second arc confirms that the polarization mechanism in IZT corresponds to bulk effect arising in semiconductive grains.

In Fig.15, the variation of normalized parameters M''/M''_{max} and Z''/Z''_{max} as a function of logarithmic frequency measured at 673 K is shown. Comparison with the impedance and electric modulus data allows the determination of the bulk response in terms of localized i.e., defect relaxation or non-localized conduction, i.e., ionic or electrical conductivity [21]. The position of the peak in the Z''/Z''_{max} is shifted towards lower frequency region in relation to the M''/M''_{max} peak. The type of dielectric response can be determined by inspection of the magnitude of overlapping between the peaks of both parameter Z″(ω) and M″(ω). The peak position of M''/M''_{max} and Z''/Z''_{max} do not overlap but are very close suggesting the components from both long-range and localized relaxation.

The dielectric constant is said to be a ground state property and can in principle be exactly calculated within DFT because the dielectric constant can be determined by taking the second derivative of the ground state energy with respect to an applied electric field. Hence, the electronic structure calculation of the material is performed in the next section to observe the electronic properties of the material. The measured structural parameters have been further be used to calculate the electronic structure of the material.

4. GROUND STATE PROPERTIES

The ground-state properties of IZT are investigated employing the FLAPW method within the generalized gradient approximation (GGA) [16]. The structural parameters of the system were optimized at 2000-k points inside the irreducible Brillouin zone for integration. The full geometrical optimization gives an in-plane lattice constant a = b = c = 8.08 $\overset{0}{A}$ and c/a = 1.0 of pure In_2ZnTiO_6. Accurate optimizations of crystal geometries have come to serve as a stringent test for electronic structure calculations. We use our optimized parameters for

the study of electronic structure calculations taking muffin tin radius (RMT) as 2.0, 1.9, 1.8 and 1.6 for In, Zn, Ti and O respectively.

In **Fig. 16**, we have shown the calculated and minimized total energy with respect to the volume. In our calculation, the crystal structure of IZT has the space group symmetry Fm-3m. The Birch-Murnaghan relation for equation of state (EOS) is used to get the static equilibrium volume V_0 (=940.39) as well as the bulk modulus B_0 (= 123.55 GPa) and its pressure derivative B' (= 3.0873) at zero pressure. The pressure derivative of bulk modulus at zero pressure B_0' is a parameter of great physical significance in high pressure physics. It is related to a few other important thermo physical properties (like phase transitions, interphase energy, adsorption energy etc.) [22].

In **Fig. 17**, the calculated band structure for IZT in the high symmetry direction in the Brillouin zone has been shown. In this figure, we find a large dispersion of the bands. It can be seen that there are many bands from –3 eV to 1 eV. These bands are mainly contributed from Ti-d and O-p electrons. These bands also overlap each other at and around the Fermi level which indicates that there is hybridization between the Ti-d and O-p states.

Fig. 18 shows the total DOS along with partial DOS of Ti-d, O-p, Zn-s and In-p states of IZT. It is observed that the main contribution in the valence band comes from Ti-3d state. The Ti-d state hybridizes with O-p states near Fermi level. In IZT the contribution of Zn-d state near Fermi level is negligible. The hybridization between Ti-d and O-p states implies that the interaction between the atoms of these two is highly covalent.

5. CONCLUSIONS

Double perovskite oxide, indium zinc titanate, $In_2(ZnTi)O_6$ (IZT) is synthesized by the solid state reaction technique. The field dependence of the conductivity and the dielectric response of the sample are measured in a frequency range from 42 Hz to 1.1 MHz and in the temperature range from room temperature to 673 K. With the increase of frequency, the dielectric constant decreases. The frequency dependence of the peak loss is found to obey an Arrhenius law with activation energy of 0.73 eV. An analysis of loss factor with frequency is performed by using the scaling behaviour of the dielectric loss spectra. The complex impedance plot of the sample confirms that the polarization mechanism in IZT corresponds to bulk effect of semiconductor. The relaxation mechanism is also discussed in the framework of impedance and modulus formalism. The full potential linearized augmented plane wave (FLAPW) method is employed to study the ground state properties of IZT. From the calculation, it is found that Ti-d state hybridizes with O-p state near Fermi level which implies that the interaction between the atoms of these two is highly covalent.

Acknowledgement: Critical comments of reviewers are gratefully acknowledged. Also, financial support rendered by DAE-BRNS, Mumbai and DST; CSIR; UGC, New Delhi is gratefully acknowledged.

REFERENCES

[1] Kobayashi, K. I., Kimura, T., Sawada, H., Terakura, K., & Tokura, Y. (1998). Room-temperature magnetoresistance in an oxide material with an ordered double-perovskite structure. *Nature*, *395*(6703), 677-680.

[2] Wolf, S. A., Awschalom, D. D., Buhrman, R. A., Daughton, J. M., von Molnár, V. S., Roukes, M. L., ... & Treger, D. M. (2001). Spintronics: a spin-based electronics vision for the future. *science*, *294*(5546), 1488-1495.

[3] Kato, H., Okuda, T., Okimoto, Y., Tomioka, Y., Takenoya, Y., Ohkubo, A., ... & Tokura, Y. (2002). Metallic ordered double-perovskite Sr 2 CrReO 6 with maximal Curie temperature of 635 K. *Applied physics letters*, *81*(2), 328-330.

[4] Borges, R. P., Thomas, R. M., Cullinan, C., Coey, J. M. D., Suryanarayanan, R., Ben-Dor, L., ... & Revcolevschi, A. (1999). Magnetic properties of the double perovskites A2FeMoO6; A= Ca, Sr, Ba. *Journal of Physics: Condensed Matter*, *11*(40), L445.

[5] Navarro, J., & Frontera, C. (2001). L1. Balcells, B. Martinez, and J. Fontcuberta. *Phys. Rev. B*, *64*, 92411.

[6] Sarma, D. D., Sampathkumaran, E. V., Ray, S., Nagarajan, R., Majumdar, S., Kumar, A., ... & Row, T. G. (2000). Magnetoresistance in ordered and disordered double perovskite oxide, Sr2FeMoO6. *Solid State Communications*, *114*(9), 465-468.

[7] Setter, N., & Cross, L. E. (1980). The contribution of structural disorder to diffuse phase transitions in ferroelectrics. *Journal of Materials Science*, *15*(10), 2478-2482.

[8] Petrova, D., Dobreva, S., Veleva, M., Macicek, J., & Gospodinov, M. (1997). Growth, structure, dielectric behavior and AC-conductivity of pyrochlore lead-scandium tantalate single crystals. *Materials research bulletin*, *32*(11), 1543-1549.

[9] M. Retuerto, J. A. Alonso, M. Garci a-Hernandez, M. J. Martinez-Lope, Solid State Communications **139**, 19 (2006).

[10] Caracas, R., & Gonze, X. (2005). First-principles determination of the dynamical properties of Pb 2 Mg Te O 6. *Physical Review B*, *71*(5), 054101.

[11] Caracas, R., & Gonze, X. (2002). First-principles study of Pb 2 MgTeO 6: High-T cubic phase and average low-T rhombohedral phase. *Physical Review B*, *65*(18), 184103.

[12] Baldinozzi, G., Sciau, P., & Buffat, P. A. (1993). Investigation of the orthorhombic structures of Pb2MgWO6 and Pb2CoWO6. *Solid state communications*, *86*(9), 541-544.

[13] Baldinozzi, G., Sciau, P., & Bulou, A. (1997). Analysis of the phase transition sequence of the elpasolite (ordered perovskite). *Journal of Physics: Condensed Matter*, *9*(47), 10531.

[14] Azad, A. K., Ivanov, S. A., Eriksson, S. G., Eriksen, J., Rundlöf, H., Mathieu, R., & Svedlindh, P. (2001). Synthesis, crystal structure, and magnetic characterization of the double perovskite Ba2MnWO6. *Materials research bulletin*, *36*(12), 2215-2228.

[15] Battle, P. D., & Jones, C. W. (1989). The crystal and magnetic structures of Sr2LuRuO6, Ba2YRuO6, and Ba2LuRuO6. *Journal of Solid State Chemistry*, *78*(1), 108-116.

[16] P. Blaha, K. Schwarz, G. Madsen, D. Kvasnicka & J. Luitz, *WIEN 2K, An Augmented Plane Wave + Local Orbitals Program for Calculating Crystal Properties* (Karlheinz Schwarz, Techn. Universitat Wien, Austria), 2001. ISBN 3 – 950103 1 – 1 – 2.

[17] Almond, D. P., & West, A. R. (1983). Anomalous conductivity prefactors in fast ion conductors. *Nature*, *306*(5942), 456-457.

[18] Hairetdinov, E. F., Uvarov, N. F., Patel, H. K., & Martin, S. W. (1994). Estimation of the free-charge-carrier concentration in fast-ion conducting Na 2 S-B 2 S 3 glasses from an analysis of the frequency-dependent conductivity. *Physical Review B*, *50*(18), 13259.

[19] Jonscher, A. K. (1999). Dielectric relaxation in solids. *Journal of Physics D: Applied Physics*, *32*(14), R57.

[20] Cole, K. S., & Cole, R. H. (1941). Dispersion and absorption in dielectrics I. Alternating current characteristics. *The Journal of chemical physics*, *9*(4), 341-351.

[21] Gerhardt, R. (1994). Impedance and dielectric spectroscopy revisited: distinguishing localized relaxation from long-range conductivity. *Journal of Physics and Chemistry of Solids*, *55*(12), 1491-1506.

[22] Almond, D. P., & West, A. R. (1983). Anomalous conductivity prefactors in fast ion conductors. *Nature*, *306*(5942), 456-457.

List of Figures

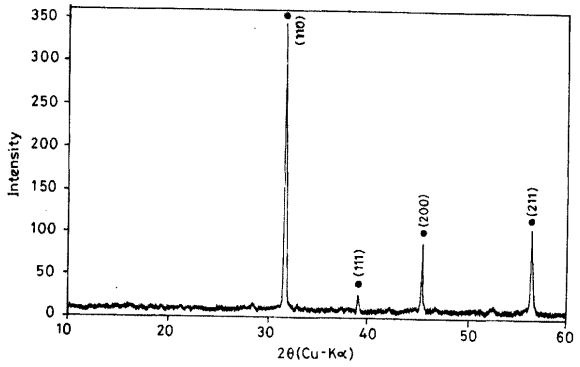

Fig.1 XRD pattern of IZT

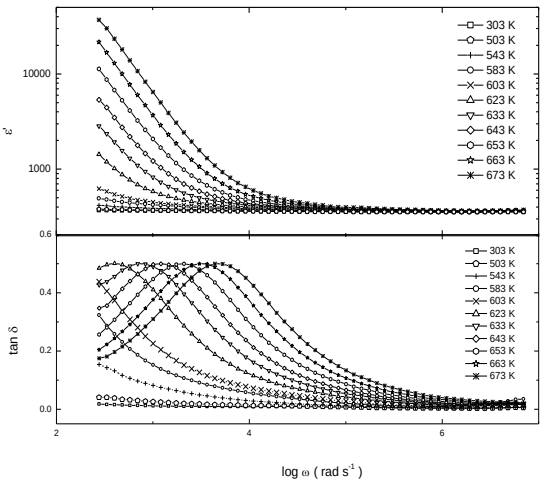

Fig 2 Frequency (angular) dependence of ε′ (a) and tan δ (b) of In_2ZnTiO_6

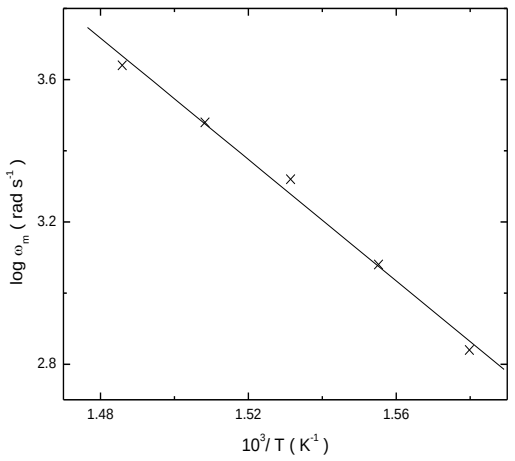

Fig 3 Temperature dependence of the most probable relaxation frequency obtained from the frequency spectra of the dielectric loss for In_2ZnTiO_6. The crosses are the experimental points and the solid line is the least-squares straight-line fit.

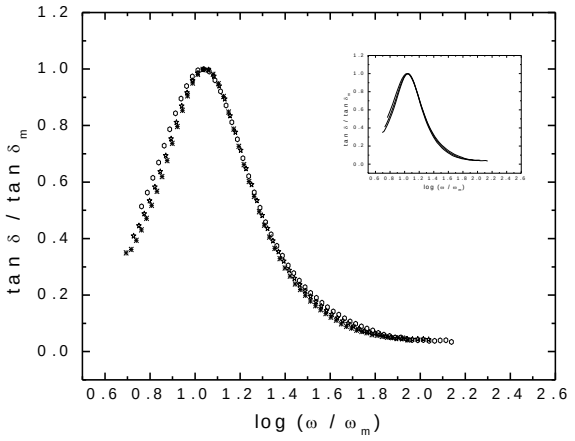

Fig 4 Scaling behaviour of dielectric loss at various temperatures for In_2ZnTiO_6

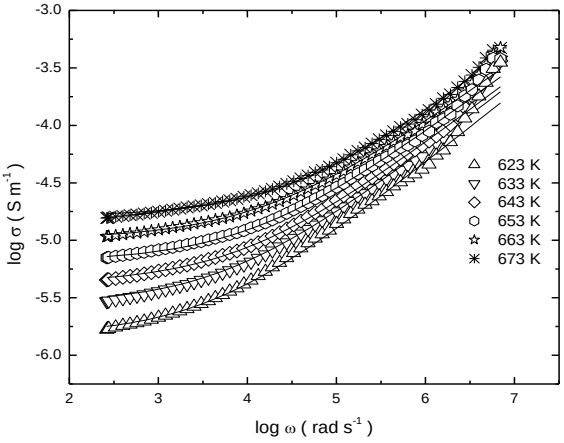

Fig 5 Frequency spectra of the conductivity for In_2ZnTiO_6 at various temperatures. The solid curves are the best fits to Eq. (2)

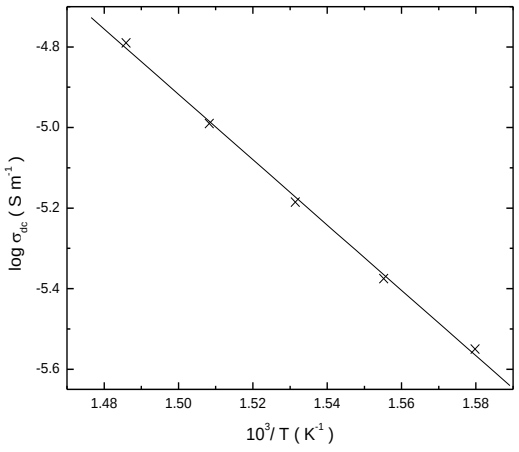

Fig 6 Temperature dependence of the dc conductivity curve for In_2ZnTiO_6. The crosses are the experimental points and the solid line is the least-squares straight-line fit.

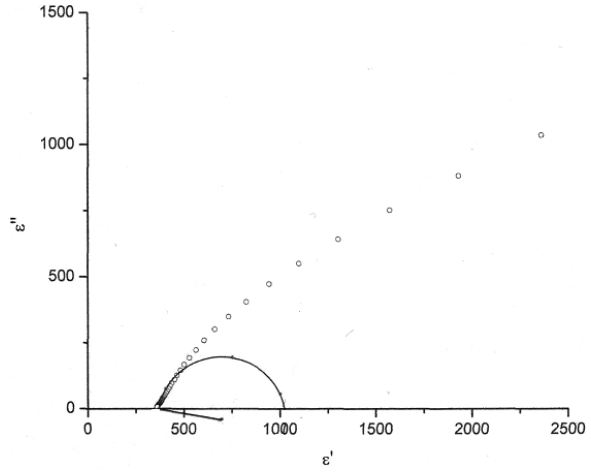

Fig 7 Complex Argand plane plot between ε″ and ε′ for In_2ZnTiO_6 at 633 K

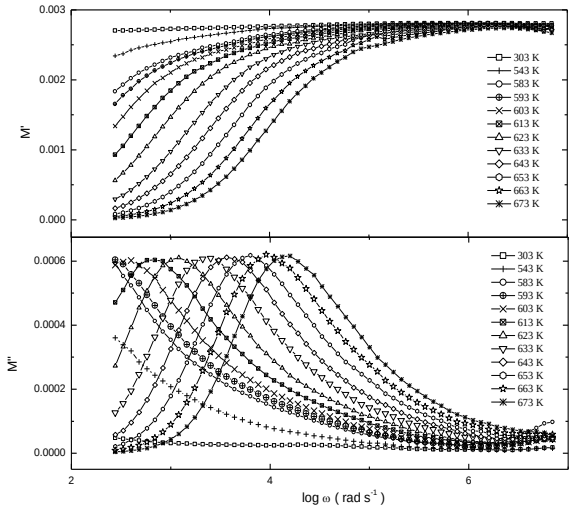

Fig 8 Frequency (angular) dependence of M′ (a) and M″ (b) of In_2ZnTiO_6 at various temperatures.

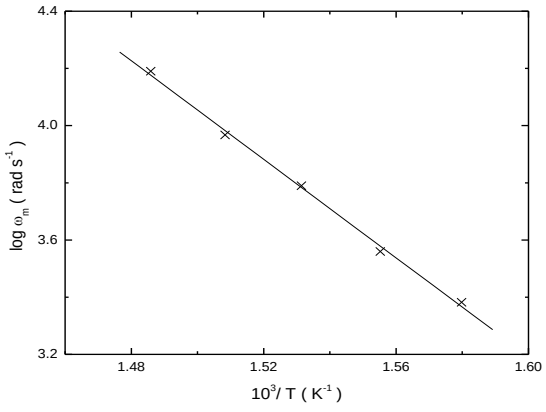

Fig 9 Temperature dependence of the most probable relaxation frequency obtained from the frequency-dependent imaginary part of the modulus curves for In_2ZnTiO_6. The crosses are the experimental points and the solid line is the least-squares straight-line fit.

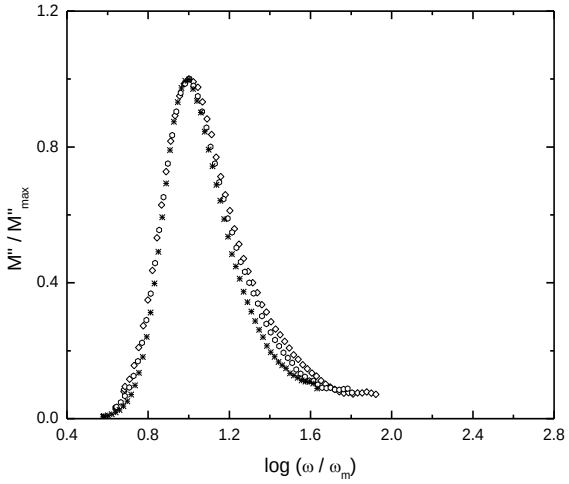

Fig 10 Scaling behaviour of M″ at various temperatures for In_2ZnTiO_6

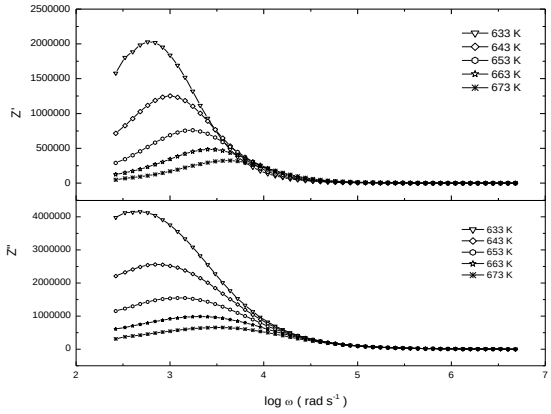

Fig 11 Frequency (angular) dependence of the Z′ (a) and Z″ (b) of In_2ZnTiO_6 at various temperatures.

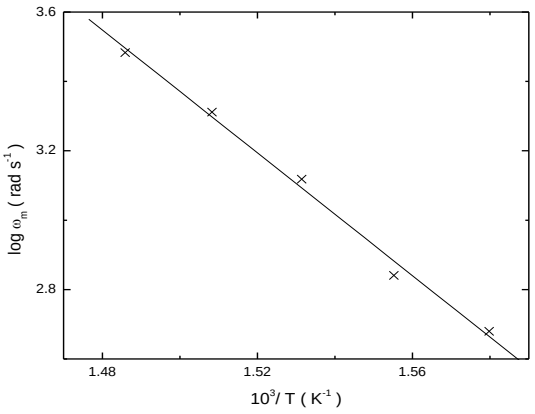

Fig 12 Temperature dependence of the most probable relaxation frequency obtained from the frequency-dependent imaginary part of the impedance curves for In_2ZnTiO_6. The crosses are the experimental points and the solid line is the least-squares straight-line fit.

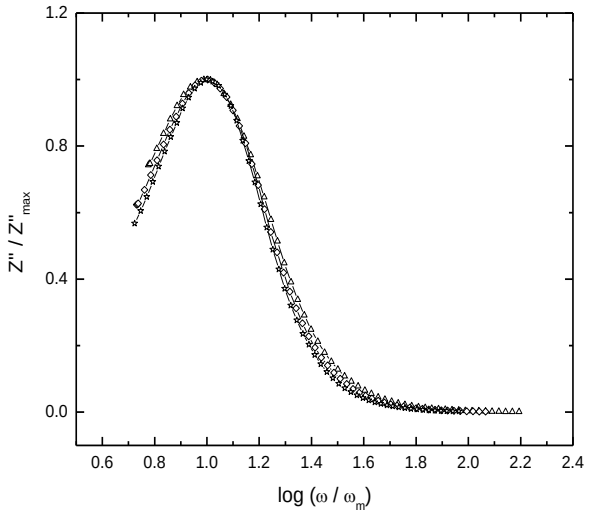

Fig 13 Scaling behaviour of Z″ at various temperatures for In_2ZnTiO_6

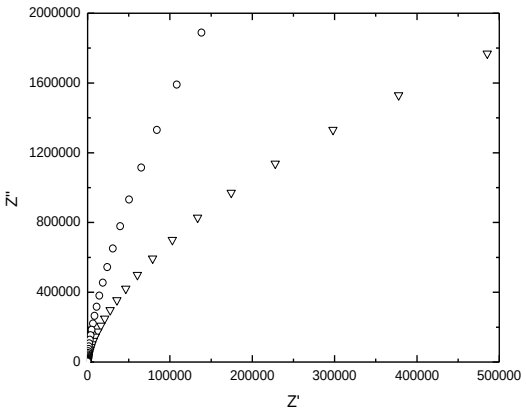

Fig 14 Complex Argand plane plot between Z″ and Z′ for In_2ZnTiO_6 at 583 K and 633 K

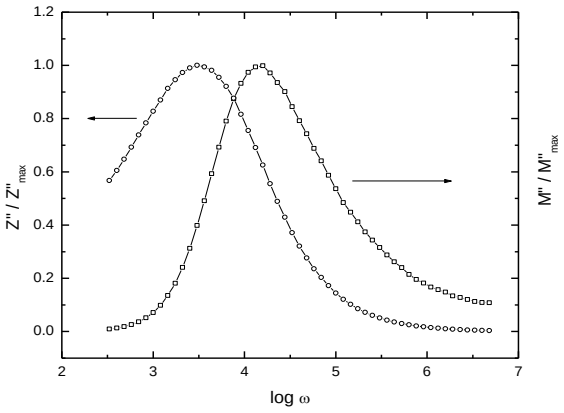

Fig 15 Frequency dependence of normalized peaks, Z″ / Z''_{max} and M″ / M''_{max} for In_2ZnTiO_6 at 673 K.

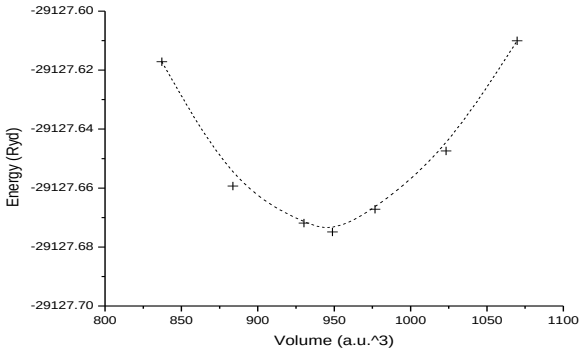

Fig. 16 Total Energy of In_2ZnTiO_6 as a function of cell volume

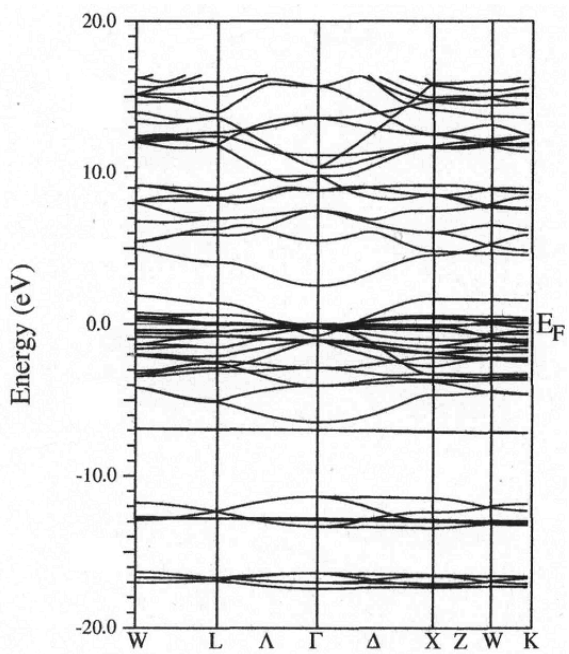

Fig. 17 The electronic band structure of In_2ZnTiO_6 along high symmetry directions

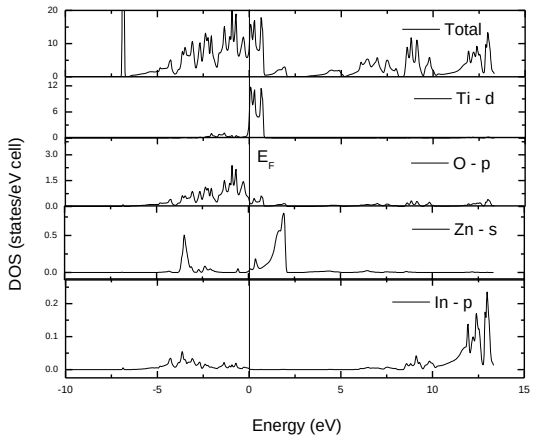

Fig. 18 Total DOS and PDOS of In_2ZnTiO_6 calculated for the optimized lattice constant

